Structure of the inhibitory receptor for human natural killer cells resembles haematopoietic receptors

Qing R. Fan*†, Lidia Mosyak*†, Christine C. Winter‡, Nicolai Wagtmann‡, Eric O. Long‡ & Don C. Wiley*

* *Department of Molecular and Cellular Biology, Howard Hughes Medical Institute, Harvard University, 7 Divinity Avenue, Cambridge, Massachusetts 02138, USA*

‡ *Laboratory of Immunogenetics, National Institute of Allergy and Infectious Diseases, National Institutes of Health, 12441 Parklawn Drive, Rockville, Maryland 20852, USA*

† *These authors contributed equally to this work.*

Abnormal cells deficient in class I major histocompatibility complex (MHC) expression are lysed by a class of lymphocytes called natural killer (NK) cells[1]. This lysis provides a defence against pathogens and tumour cells that downregulate MHC expression to avoid an MHC-restricted, T-cell immune response. Normal cells escape lysis because their MHC molecules are recognized by NK-cell inhibitory receptors, which inhibit lysis[2]. Several such inhibitory receptor families have been described in humans and mice (reviewed in ref. 2). In the human killer-cell inhibitory receptor family, individual p58 members are specific for a subset of class I human leukocyte antigen (HLA)-C molecules. The human p58 natural killer-cell inhibitory receptor clone 42 recognizes HLA-Cw4, -Cw2, -Cw5 and -Cw6, but not HLA-Cw3, -Cw1, -Cw7 or -Cw8, which are recognized by p58 killer-cell inhibitor receptor clone 43 (ref. 3). We have determined the X-ray structure of the p58 NK-cell inhibitory receptor clone 43 at 1.7-Å resolution. The structure has tandem immunoglobulin-like domains positioned at an acute, 60-degree angle. Loops on the outside of the elbow between the domains form a binding site projected away from the NK-cell surface. The topology of the domains and their arrangement relative to each other reveal a relationship to the haematopoietic receptor family, with implications for the signalling mechanism in NK cells.

The soluble ectodomain of the p58 natural killer-cell inhibitory receptor (KIR) that we crystallized was expressed in bacteria and refolded *in vitro*[4]. It specifically blocks the binding of a KIR–immunoglobulin fusion protein to cells expressing HLA-Cw4, but has no effect on the binding of a KIR–immunoglobulin fusion protein specific for HLA-CW3 to cells expressing HLA-CW3 (ref. 4). The entire KIR ectodomain, residues 1–224, and a shorter form, residues 1–200, without the stem domain of 24 residues, were both shown by a gel-shift assay to bind to soluble, recombinant HLA-Cw4 (ref. 4). As predicted from sequence similarity[5], the overall fold of each KIR domain resembles immunoglobulin-like domains containing two antiparallel β-sheets[6] (Fig. 1a, b). Topologically, the p58 KIR structure has tandem fibronectin type III-like domains, which are structurally similar to immunoglobulin domains. The two domains are equal in size (domain D1, residues 6–101; domain D2, residues 105–200), and are connected by a three-residue linker (residues 102–104) (Fig. 1b).

The topology of the D1 immunoglobulin-like domain is of the h-type[6], similar to that of the D1 domains of the human growth hormone receptor (hGHR)[7], human prolactin receptor (hPLR)[7], and the erythropoietin receptor (EPOR)[8]. The D2 domain has the closely related s-type topology[6] found in the D2 domains of hGHR, hPLR and EPOR[8–10], and both domains of class II receptors of the haematopoietic superfamily, including the α-chain of the interferon-γ receptor (IFN-γRα)[11], and tissue factor[12,13]. The s-type topology has also been found in other two-domain structures, including the co-receptor CD4 (refs 14, 15), the cell-adhesion molecule CD2 (ref. 16) and neuroglian[17]. However, in both CD2 and CD4, the s-type domain is paired in tandem with a variable-type immunoglobulin domain and the two domains assume a linear conformation, lacking the elbow region found in all of the haematopoietic receptors and KIR. Although some members of the haematopoietic receptor superfamily contain additional domains, ligand binding is mediated through the h- or s-type domains[7]. The s-type topology of D2 has a β-sheet of three strands, A, B and E (Fig. 1a, b, dark orange) packed against a β-sheet of four strands, C′, C, F and G (Fig. 1a, b, light orange). In h-type topology of the D1 domain, the C′ strand is elongated, pairing first with the C strand of the C′CFG β-sheet and at its far end (where it is renamed D) pairing with the E strand of the ABE(D) β-sheet (Fig. 1a, b). The switch from one β-sheet to the other occurs at a kink in strand C′/D at Gly 53. When superimposed, the D1 and D2 domains, which have 40% sequence identity, are strikingly similar in structure with a root-mean-square (r.m.s.) deviation of 0.9 Å for 85 Cα pairs.

Table 1 Statistics for data collection and refinement

Data collection

Data set	Wavelength (Å)	Scattering factors (e)		Resolution (Å)	Unique reflections	Average $I/\sigma(I)$	Completeness (%)	R_{sym} (%)†
		f'	f''					
MAD	0.9639 (remote)	−3.49	3.72	10.0–2.2	11,480	18.9	98.7 (99.1)	7.3 (11.7)
	0.9791 (peak	−7.89	4.72	10.0–2.2	11,449	18.5	98.6 (99.1)	7.2 (11.6)
	0.9794 (edge)	−9.86	3.05	10.0–2.2	11,495	18.8	98.8 (99.1)	7.0 (11.3)
native	0.918			16.0–1.7	25,065	17.1	99.6 (97.8)	7.3 (23.4)

Refinement (6–1.7 Å)

				R.m.s. deviations		
R_{cryst} (R_{free})‡ (%)	Reflections (free)	Non-hydrogen protein atoms	solvent molecules	Bonds (Å)	Angles (°)	B-factors (Å^2)
20.6 (25.6)	24,473 (2,427)	1,513	211	0.010	1.83	2.85

Values in parentheses correspond to the last resolution shell; 2.28–2.20 Å for MAD data sets, or 1.76–1.70 Å for native data set.

* The values of f' and f'' for λ_{peak} and λ_{edge} were derived from the experimental values of the absorption spectrum; values for λ_{remote} were calculated form theoretical cross-sections[30].

† $R_{sym} = \Sigma|I_i - \langle I\rangle|/\Sigma I_i$, where I_i is the intensity of an individual reflection, and $\langle I\rangle$ is the average intensity of that reflection. Bijvöet mates were considered as separate reflections.

‡ $R_{cryst} = \Sigma||F_p| - |F_c||/\Sigma|F_p|$, where F_c is the calculated structure factor. R_{free} is equivalent to R_{cryst}, but calculated for a randomly chosen 10% of reflections that were omitted from the refinement process.

KIR domains define a new topological subtype[6], which we call Kh- and Ks-type, in which the carboxy-terminal half of strand A, named A′, pairs with strand G to form a five-stranded sheet C′CFGA′ (Fig. 1a, b, light orange) by switching at *cis* prolines (residues 14 and 114) from one β-sheet to another, as found in variable domains of antibody light chains, CD8 and T-cell antigen receptors.

A signature sequence motif of class I haematopoietic receptors, the WSXWS box[18], is also present in p58 KIR. The p58 clone 42 KIR (p58-cl42) contains at residues 188–192 a variant of the WSXWS sequence motif (WSKSS) in D2, in the same location as found in the haematopoietic receptor family (Fig. 1a, b). Like the motif in the other structures, the WSKSS sequence in KIR assumes a polyproline type II conformation, resulting in a wide β-bulge[8–10] in which the hydroxyl groups of the two conserved serine residues (underlined) form hydrogen bonds to the adjacent F-strand backbone, replacing the usual backbone-to-backbone hydrogen bonds between strands in a β-sheet. A surface cluster of aromatic and charged side chains near the motif present in several haematopoietic receptors[8–10] is absent in KIR. KIR differs from members of the haematopoietic receptor superfamily in that a variant of the motif also occurs in D1 (Fig. 1a, b). The sequence VSAPS, residues 90–94, forms the same type of β-bulge at the homologous position. Variants of both the V SAPS and WSKSS sequences are found in the sequences of all KIR immunoglobulin-like domains, with the two structurally important serines completely conserved.

Helical linkers of at least four residues in length have been found linking the D1 and D2 domains in five members of the haematopoietic receptor family: hGHR, hPLR, EPOR, IFN-γRα and tissue factor[8–13]. The D1 and D2 domains of the KIR are more tightly connected by a three-residue linker (residues 102–104) with a helical conformation ($\phi = -95.7$ deg, $\psi = -18.4$ deg) at Leu 104.

Most of the side chains in the D1–D2 interface are conserved in all KIR sequences, and the few differences there are appear consistent with the observed packing, suggesting that the V shape will be a feature of all p58 and p70 KIRs. Extensive hydrogen bonding between strands of both domains and the large buried solvent-accessible surface area, 1,076 Å^2 (calculated using the program SURFACE[19]; probe radius 1.4 Å), suggest that the elbow angle is fixed. The D1–D2 interface includes a three-stranded parallel β-sheet formed by the two strands A′ and G from the D1 domain and a short segment of strand G in the D2 domain (Fig. 1a, b). D1–D2 contacts occur not only at the tip of the V (Fig. 2a, black) but also across the gap between the arms of the V (Fig. 2a, red). Most of the polar interactions found at the interface involve main-chain atoms, and are therefore independent of sequence variation.

Site-directed mutations indicate strongly that the binding site on

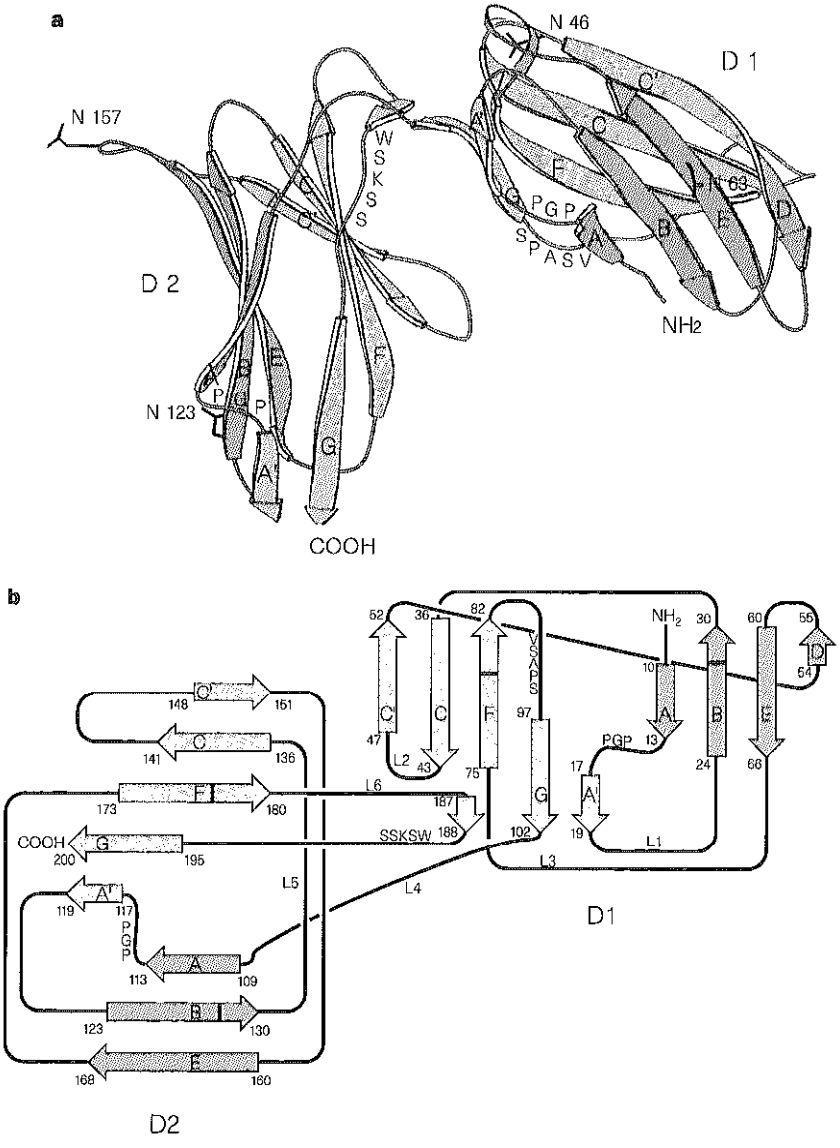

Figure 1 Structure and topology of p58-cl42 KIR. **a**, KIR domain D1 is N-terminal, and D2 is C-terminal; ABED β-sheet (dark orange) and C′CFGA′β-sheet (light orange); WSKSS and VSAPS motifs (red); potential glycosylation sites at asparagines 46, 63, 123 and 157 (black). **b**, Topological diagram showing the h-type immunoglobulin-like fold of D1 and the s-type fold of D2. The β-sheet at the D1–D2 interface (strands A′ and G in D1 and a fragment of strand G in D2) is shown below D1. Loops L1–L6 are implicated in ligand binding by the haematopoietic receptors, hGHR, hPLR and EPOR. Cysteines 28, 79, 128 and 177 are indicated by black bars.

p58-cl42 for its HLA ligand includes Met 44 (ref. 20) on the C–C′ loop that projects from the elbow between D1 and D2 (Fig. 2b, red star; Fig. 1b, L2). Exchanging Met 44 in p58-cl42 with lysine, found at that position in p58-cl43, switched the specificity of p58-cl42 from HLA-Cw4 to HLA-Cw3, and vice versa[20]. Of the six ligand-binding loops of class I haematopoietic receptors (L1–L6 in Fig. 1b), sequence variation among KIRs (Fig. 2b) implicates at least three in ligand binding (L2, L3 and L6 in Fig. 1b). Loops at the elbow between domains contact ligand in the 1 : 1 complex of human prolactin receptor (hPLR) (Fig. 3c, green) with growth hormone (hGH) (orange).

In contrast to the 'elbow angles' found in the haematopoietic receptors, which are 90 deg for hGHR, EPOR and hPLR and 120 deg for IFN-γRα and tissue factor, the interdomain angle in KIR is 60 deg (compare Fig. 3a, b). The KIRs may thus define a new structural class of receptors, related to the haematopoietic receptor family that binds soluble ligands, but adapted, through the acute interdomain angle, to bind to membrane-bound ligands during cell–cell interactions that result in signalling.

The KIR binding site on class I MHC molecules has been mapped to the α1 domain (reviewed in ref. 2). Residues in the region of the C-terminal end of the α1-domain α helix, and on the loop following it in the sequence (Fig. 3e, red), have been identified as part of the site on HLA-C and HLA-B molecules recognized by p58 and p70 KIRs. The inhibitory signal delivered by KIR after binding an MHC molecule is initiated by the phosphorylation of its cytoplasmic ITIM motif which, in turn, binds to the Src-homology 2 (SH2) domains of the tyrosine phosphatase SHP-1, thereby both recruiting it to the membrane and revealing its phosphatase activity[21,22]. This mechanism requires the recruitment of a protein tyrosine kinase to phosphorylate the KIR ITIM following KIR–MHC binding.

By analogy to the haematopoietic receptors, KIR signalling following ligand binding might be expected to involve either dimerization of KIR or binding to another polypeptide chain[7,23]. Formation of a homodimer would be expected to bring the cytoplasmic domains of KIR into close proximity, which may facilitate phosphorylation of the ITIM motif by a cytoplasmic kinase, as in the case of the hGHR and EPOR[23]. Alternatively, formation of a heterodimer of KIR with another polypeptide that contains an associated kinase (covalently or non-covalently linked) could lead directly to phosphorylation of the KIR ITIM, as in the case of the interleukin (IL)-3/granulocyte macrophage colony-stimulating factor/IL-5 and IL-6 receptors[23]. It is possible that after binding an MHC molecule, a p58 KIR may heterodimerize with a p50 form of the KIR family, which, because of their potential to deliver positive signals[24], might be able to recruit a tyrosine kinase to the ITIM of an HLA-bound p58-KIR.

By analogy to hGHR and EPOR (Fig. 3d), dimerization of KIR might be expected to involve pairing of D2 domains (shown schematically in Fig. 3e). Disulphide-linked dimers have been observed in one group of p70 KIR[25] that are probably linked through a cysteine corresponding to position 220 in the p58 KIR stem segment following D2, which favours dimerization through D2. The existence of preformed p70 KIR dimer before ligand binding

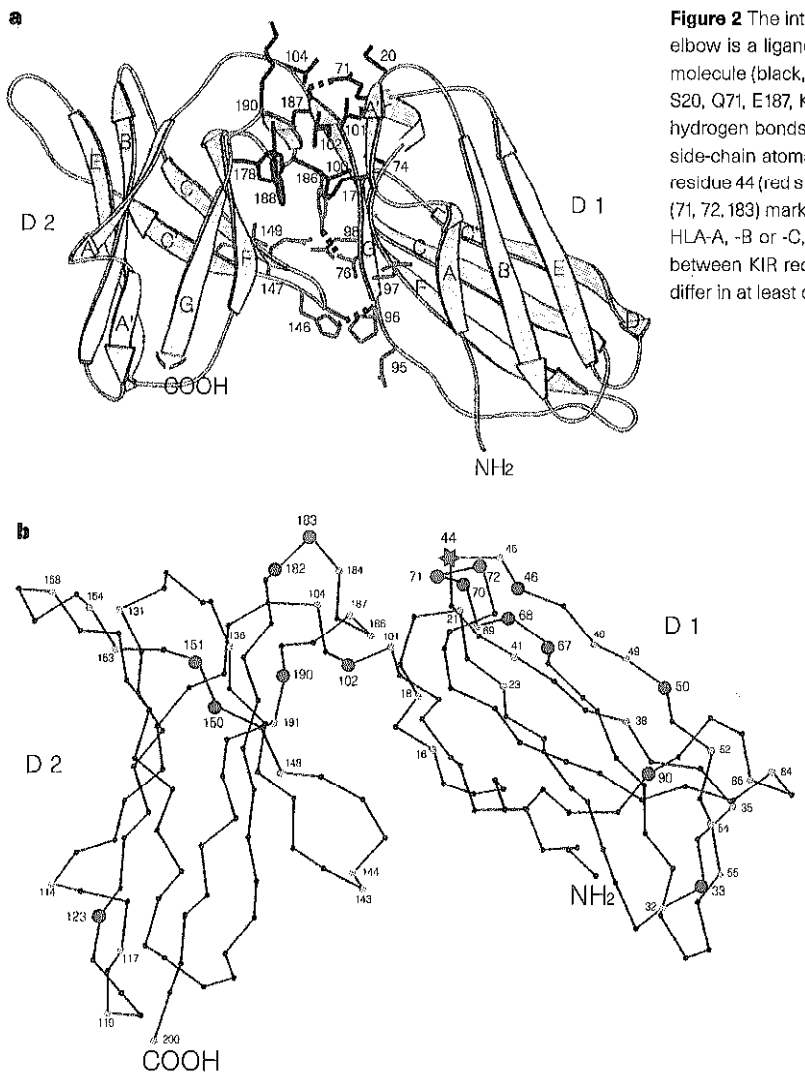

Figure 2 The interdomain interface defines a 60-deg angle and the interdomain elbow is a ligand-binding site. **a**, Non-polar contacts at the tip of the V-shaped molecule (black, V100, I102, L17, P178, W188, A74, I101, I104 and aliphatic parts of S20, Q71, E187, K190) and across the arms of the V (red). Of the 11 interdomain hydrogen bonds, 8 include β-sheet main-chain atoms (not shown); 3 use some side-chain atoms (P96–H146, Y186–T76, E187–N71; dotted lines). **b**, Exchanging residue 44 (red star) changes the specificity from HLA-Cw4 to HLA-Cw3. Red dots (71, 72, 183) mark positions that are conserved within subsets of KIR recognizing HLA-A, -B or -C, but are different in each KIR subset. Blue dots mark variation between KIR recognizing HLA-Cw4 and HLA-Cw3. Positions with orange dots differ in at least one KIR sequence.

indicates that the signalling mechanism, at least of that KIR, may involve molecules other than a putative receptor dimer. The stem region of KIR may contribute to HLA binding (Q.R.F. *et al.*, unpublished data). The full ectodomain of p58-cl42 KIR (residues 1–224) completely blocked the binding of the shorter form (residues 1–200 lacking the stem segment) to soluble HLA-Cw4 on band-shift assays (data not shown). Furthermore, binding of the shorter form to HLA-Cw4 was reversed upon addition of the longer form, suggesting a higher dissociation constant for the complex between HLA-Cw4 and the shorter form. The more favourable binding observed between HLA-Cw4 and the KIR that includes the stem (residues 220–224) suggests a role for the C-terminal stem in ligand binding, possibly by stabilizing dimerization (Fig. 3e), considering the distance between the C terminus and the ligand-binding site (Fig. 2b).

The second receptor polypeptide chain that we postulate may bind in either a homodimer or heterodimer to a KIR–MHC complex (Fig. 3e) is expected, by analogy to the haematopoietic receptors: to have a much lower affinity for HLA, and bind only after the first KIR has bound; to bind to a second, as-yet undiscovered, site on MHC molecules; and to interact with the first KIR polypeptide at some as-yet undiscovered site, probably in the D2 domain. In the haematopoietic receptors, the affinity of the second receptor chain to the single-receptor/ligand complex is 500- to 1,000-fold weaker than the first, making detection and characterization of the second binding sites difficult[7]. This may account for the current lack of evidence for KIR dimerization by MHC molecules. □

Methods

Incorporation of Se-Met. The selenomethionyl (Se-Met) p58-cl42 KIR (residues 1–200) was expressed in *Escherichia coli* as inclusion bodies, refolded by dilution, and purified following the same procedure as native p58-cl42 (ref. 4). The incorporation of Se-Met was achieved by growing the cells in minimal medium (M9) supplemented with 2 mM $MgSO_4$, 0.1 mM $CaCl_2$, 0.2% glucose, 0.00005% thiamine, and 40 mg l^{-1} each of all L-amino acids except Cys and Met, and inducing the cells in the presence of 120 mg l^{-1} of Se-Met along with 100 mg l^{-1} each of Thr, Lys and Phe, and 50 mg l^{-1} each of Leu, Ile and Val. All

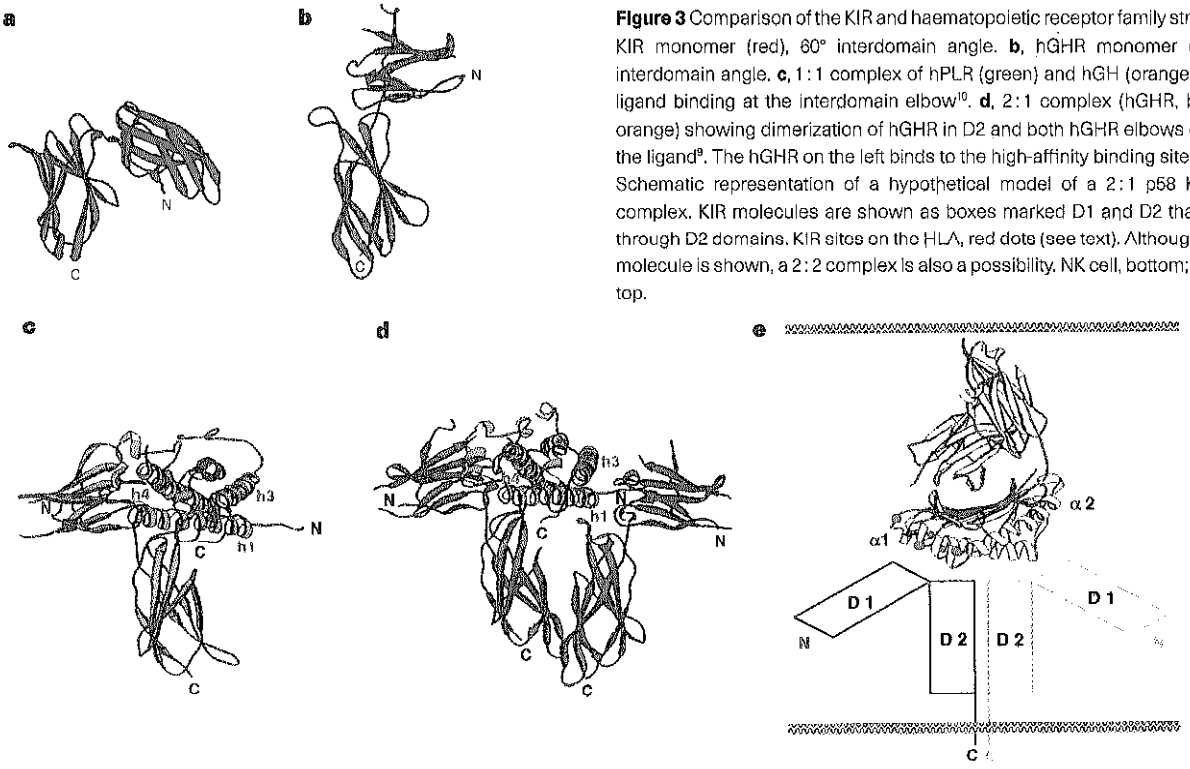

Figure 3 Comparison of the KIR and haematopoietic receptor family structures. **a**, KIR monomer (red), 60° interdomain angle. **b**, hGHR monomer (blue), 90° interdomain angle. **c**, 1:1 complex of hPLR (green) and hGH (orange), showing ligand binding at the interdomain elbow[10]. **d**, 2:1 complex (hGHR, blue; hGH, orange) showing dimerization of hGHR in D2 and both hGHR elbows contacting the ligand[9]. The hGHR on the left binds to the high-affinity binding site of hGH. **e**, Schematic representation of a hypothetical model of a 2:1 p58 KIR/HLA-C complex. KIR molecules are shown as boxes marked D1 and D2 that dimerize through D2 domains. KIR sites on the HLA, red dots (see text). Although one HLA molecule is shown, a 2:2 complex is also a possibility. NK cell, bottom; target cell, top.

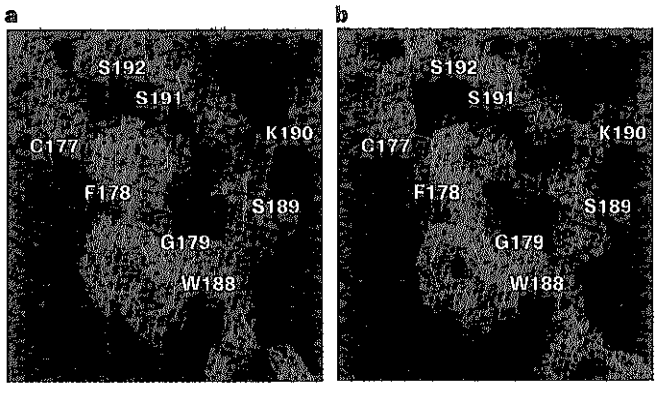

Figure 4 Electron-density maps showing the refined model in the region of the WSKSS sequence. **a**, A 2.2-Å resolution Fourier map calculated with MAD phases improved by density modification. **b**, A 1.7-Å resolution simulated-annealing-omit map calculated with the $2F_{obs} - F_{calc}$ amplitudes and model phases. Both maps are contoured at 1.2σ level.

five Met were substituted with Se-Met as determined by mass spectrometry.

Crystallization. Crystals of p58-cl42 were grown from 0.55 M $(NH_4)_2HPO_4$, 50 mM sodium citrate, pH 5.4, final pH 7.7. Hexagonal rods ($0.1 \times 0.1 \times 1.5\,mm^3$; space group $P6_1$; $a = b = 92.4$ Å, $c = 46.8$ Å; 1 molecule per asymmetric unit) grow two weeks after seeding. Se-met p58 crystallized under the same condition using the native crystals as seeds; the difference in cell dimensions was less than 0.5%. After the crystals were stabilized for at least 10 h in a harvesting solution (1.5 M $(NH_4)_2HPO_4$, 50 mM sodium citrate, pH 5.4, final pH 7.7), they were soaked for 2–5 min in a cryo-protecting solution (1.5 M $(NH_4)_2HPO_4$, 50 mM Na citrate, pH 5.4, 25% glycerol, final pH 7.7), and flash-cooled with liquid nitrogen.

Data collection. Multiwavelength anomalous dispersion (MAD)[26] data were collected to 2.2 Å with a 300-mm diameter MAR Research image-plate system at the X25 beamline of the National Synchrotron Light Source, Brookhaven National Laboratory. A high-resolution native data set was collected to 1.7 Å on the Princeton 2K CCD detector at F-1 beamline of the Cornell High Energy Synchrotron Source (CHESS). Data were processed (Table 1) using DENZO and SCALEPACK (HKL Research). Most of the subsequent processing used the CCP4 programs[19].

MAD phasing. MAD phasing was treated as a case of multiple isomorphous replacement[27]. Four selenium sites were identified from anomalous and dispersive difference Pattersons and were checked by difference Fouriers. The N-terminal methionine was disordered. Refinement of anomalous scatterer parameters and phase calculation were performed with MLPHARE[28]. Because of discrepancies between phasing statistics generated by MLPHARE and other programs[27], electron-density maps before and after model refinement are displayed instead of experimental phasing statistics (Fig. 4). The initial MAD map was improved by density modification using DM[19], assuming 40% solvent content. The correct space-group enantiomer $P6_1$ was identified by the presence of clear solvent boundary in the 2.2-Å electron-density maps.

Model refinement. The experimental MAD phases were used with the native data set to calculate the electron density for the native structure. Both density-modified and unmodified electron-density maps were used to build an 85% complete model with O (DATAONO AB). For refinement, data with $|F_{obs}| > 0$ were included. The model was initially refined at 10–2.2 Å using positional refinement and simulated annealing protocols in X-PLOR[29]. Several cycles of manual refitting and subsequent inclusion of lower-resolution data to 16 Å combined with bulk solvent correction allowed the missing loop regions to be traced. The resolution was then extended in one step to 1.7 Å. Refinement at this stage involved simulated annealing followed by *B*-factor refinement, with the extensive use of simulated annealing omit maps (Fig. 4b). The final model refined in X-PLOR contained residues 6–200 and 211 water molecules. This model was refined with REFMAC[19] (Table 1). The maximum-likelihood method in REFMAC lowered the *R*-values in the highest resolution shell (from 38.4 to 33.7% for R_{free} at 1.76–1.7 Å). All ϕ and ψ angles lie in the allowed regions of the Ramachandran plot, with 92% in the most favourable regions. Side-chain densities are well defined for all residues except 151–153 in a loop, which have *B*-factors >70 Å^2.

Figure preparation. Figures 1a, 2 and 3 were prepared using the program RIBBONS[30].

Received 27 May; accepted 3 July 1997.

1. Ljuggren, H. G. & Karre, D. In search of the "missing self": MHC molecules and NK cell recognition. *Immunol. Today* **11**, 237–244 (1990).
2. Lanier, L. L. Natural killer cells: from no receptors to too many. *Immunity* **6**, 371–378 (1997).
3. Long, E. O. *et al.* Killer cell inhibitory receptors: diversity, specificity, and function. *Immunol. Rev.* **155**, 135–144 (1997).
4. Fan, Q. R. *et al.* Direct binding of a soluble natural killer cell inhibitory receptor to a soluble human leukocyte antigen-Cw4 class I major histocompatibility complex molecule. *Proc. Natl Acad. Sci. USA* **93**, 7178–7183 (1996).
5. Wagtmann, N. *et al.* Molecular clones of the p58 natural killer cell receptor reveal Ig-related molecules with diversity in both the extra- and intracellular domains. *Immunity* **2**, 439–449 (1995).
6. Bork, P., Holm, L. & Sander, C. The immunoglobulin fold: structural classification, sequence patterns and common core. *J. Mol. Biol.* **242**, 309–320 (1994).
7. Kossiakoff, A. A. *et al.* Comparison of the intermediate complexes of human growth hormone bound to the human growth hormone and prolactin receptors. *Protein Sci.* **3**, 1697–1705 (1994).
8. Livnah, O. *et al.* Functional mimicry of a protein hormone by a peptide agonist: the EPO receptor complex at 2.8 Å. *Science* **273**, 464–471 (1996).
9. De Vos, A. M., Ultsch, M. & Kossiakoff, A. A. Human growth hormone and extracellular domain of its receptor: crystal structure of the complex. *Science* **255**, 306–312 (1992).
10. Somers, W., Ultsch, M., De Vos, A. M. & Kossiakoff, A. A. The X-ray structure of a growth hormone–prolactin receptor complex. *Nature* **372**, 478–481 (1994).
11. Walter, M. R. *et al.* Crystal structure of a complex between interferon-γ and its soluble high-affinity receptor. *Nature* **376**, 230–235 (1995).
12. Muller, Y. A., Ultsch, M. H., Kelly, R. F. & De Vos, A. M. Structure of the extracellular domain of human tissue factor: location of the factor VIIa binding site. *Biochemistry* **33**, 10864–10870 (1994).
13. Harlos, K. *et al.* Crystal structure of the extracellular region of human tissue factor. *Nature* **370**, 662–666 (1994).
14. Wang, J. *et al.* Atomic structure of a fragment of human CD4 containing two immunoglobulin-like domains. *Nature* **348**, 411–418 (1990).
15. Ryu, S. *et al.* Crystal structure of an HIV-binding recombinant fragment of human CD4. *Nature* **348**, 419–426 (1990).
16. Jones, E. Y., Davis, S. J., Williams, A. F., Harlos, K. & Stuart, D. I. Crystal structure at 2.8 Å resolution of a soluble form of the cell adhesion molecule CD2. *Nature* **360**, 232–239 (1992).
17. Huber, A. H., Wang, Y. E., Bieber, A. J. & Bjorkman, P. J. Crystal structure of tandem type III fibronectin domains from *Drosophila* neuroglian at 2.0 Å. *Neuron* **12**, 717–731 (1994).
18. Bazan, J. F. Structural design and molecular evolution of a cytokine receptor family. *Proc. Natl Acad. Sci. USA* **87**, 6934–6938 (1990).
19. Collaborative computational project No. 4. The CCP4 suite: Programs for protein crystallography. *Acta Crystallogr. D* **50**, 760–776 (1994).
20. Winter, C. C. & Long, E. O. A single amino acid in the p58 killer cell inhibitory receptor controls the ability of NK cells to discriminate between the two groups of HLA-C allotypes. *J. Immunol.* **158**, 4026–4028 (1997).
21. Burshtyn, D. N. *et al.* Recruitment of tyrosine phosphatase HCP by the killer cell inhibitory receptor. *Immunity* **4**, 77–85 (1996).
22. Binstadt, B. A. *et al.* Sequential involvement of Lck and SHP-1 with MHC-recognizing receptors on NK cells inhibits FcR-initiated tyrosine kinase activation. *Immunity* **5**, 629–638 (1996).
23. Ihle, J. N., Witthuhn, B. A., Quelle, F. W., Yamamoto, K. & Silvennoinen, O. Signaling through the hematopoietic cytokine receptors. *Annu. Rev. Immunol.* **13**, 369–398 (1995).
24. Biassoni, R. *et al.* The human leukocyte antigen (HLA)-C-specific "activatory" or "inhibitory" natural killer cell receptors display highly homologous extracellular domains but differ in their transmembrane and intracytoplasmic portions. *J. Exp. Med.* **183**, 645–650 (1996).
25. Pende, D. *et al.* The natural killer cell receptor specific for HLA-A allotypes: a novel member of the p58/p70 family of inhibitory receptors that is characterized by three immunoglobulin-like domains and is expressed as a 140-kD disulfide-linked dimer. *J. Exp. Med.* **184**, 505–518 (1996).
26. Hendrickson, W. A. Determination of macromolecular structures from anomalous diffraction of synchrotron radiation. *Science* **254**, 51–58 (1991).
27. Ramakrishnan, V. & Biou, V. Treatment of MAD data as a special case of MIR. *Meth. Enzymol.* **276**, 538–557 (1996).
28. Otwinowski, Z. *Isomorphous Replacement and Anomalous Scattering* (Daresbury Laboratory, UK, 1991).
29. Brünger, A. T. *X-PLOR, Version 3.1: A System for X-ray and NMR* (Yale Univ. Press, New Haven, CT, 1992).
30. Carson, M. Ribbon models of macromolecules. *J. Mol. Graph.* **5**, 103–106 (1987).
31. Cromer, D. T. Calculation of anomalous scattering factors at arbitrary wavelengths. *J. Appl. Crystallogr.* **16**, 437 (1983).

Acknowledgements. We thank D. N. Garboczi, X. D. Zhang, P. Rosenthal, K. Smith and L. Chen for help with data collection; R. Hellmiss for preparing Fig. 1b; W. I. Weis and V. Ramakrishnan for discussion; Y. Liu for the program for calculating *f'* and *f''* values; W. Kossiakoff for the coordinates of the hPLR–hGH complex; Harvard microchemistry facility for mass spectroscopy; A. Haykov and R. Crouse for technical support; the staff at the Brookhaven X25 beamline and CHESS for assistance with data collection; and D. N. Garboczi for reading the manuscript. Q.R.F. is a recipient of an NSF predoctoral fellowship. L. M. is an associate and D. C. W. is an investigator of the Howard Hughes Medical Institute.

Correspondence and requests for materials should be addressed to D.C.W. (e-mail: wiley@crystal.harvard.edu). Coordinates will be deposited in the Brookhaven Data base and are available now from Q.R.F. (e-mail: fan@crystal.harvard.edu).